
A FORWARD SENSITIVITY APPROACH FOR ESTIMATING EDDY VISCOSITY CLOSURES IN NONLINEAR MODEL REDUCTION

A PREPRINT

Shady E. Ahmed

School of Mechanical & Aerospace Engineering,
Oklahoma State University,
Stillwater, OK 74078, USA.
shady.ahmed@okstate.edu

Kinjal Bhar

School of Mechanical & Aerospace Engineering,
Oklahoma State University,
Stillwater, OK 74078, USA.
kbhar@okstate.edu

Omer San

School of Mechanical & Aerospace Engineering,
Oklahoma State University,
Stillwater, OK 74078, USA.
osan@okstate.edu

Adil Rasheed

Department of Engineering Cybernetics,
Norwegian University of Science and Technology,
N-7465, Trondheim, Norway.
adil.rasheed@ntnu.no

ABSTRACT

In this paper, we propose a variational approach to estimate eddy viscosity using forward sensitivity method (FSM) for closure modeling in nonlinear reduced order models. FSM is a data assimilation technique that blends model's predictions with noisy observations to correct initial state and/or model parameters. We apply this approach on a projection based reduced order model (ROM) of the one-dimensional viscous Burgers equation with a square wave defining a moving shock. We investigate the capability of the approach to approximate an optimal value for eddy viscosity with different measurement configurations. Specifically, we show that our approach can sufficiently assimilate information either through full field or sparse field noisy measurements to estimate eddy viscosity closure to cure standard Galerkin reduced order model (GROM) predictions. Therefore, our approach provides a modular framework to correct forecasting error from a sparse observational network on a latent space. We highlight that the proposed GROM-FSM framework is promising for emerging digital twin applications, where real-time sensor measurements can be used to update and optimize surrogate model's parameters.

Keywords Forward sensitivity method, Galerkin projection, proper orthogonal decomposition, reduced order modeling, closure modeling, moving shock, Burgers equation

1 Introduction

Data assimilation (DA) is a family of algorithms and techniques that aim at blending mathematical models with (noisy) observations to provide better predictions by correcting initial condition and/or model's parameters [1–3]. DA plays a key role in geophysical and meteorological sciences to make more reliable numerical weather predictions. Standard popular algorithms that are often adopted in weather prediction centers include variational methods (e.g., 3D-VAR [4, 5] and 4D-VAR [6–11] methods), sequential methods (e.g., reduced rank (ensemble) Kalman filters [12–19]), and hybrid methods [20–26]. Another method that mitigates the computational cost in solving the inherent optimization problem in variational methods is called the forward sensitivity method (FSM) developed by Lakshminarayanan and Lewis [27, 28]. FSM builds on the assumption that model error stems from incorrect specification of the control elements, which include initial conditions, boundary conditions, and physical/empirical parameters. The FSM approach corrects the control elements using information from the time evolution of sensitivity functions, defined as the derivatives of model output with respect to the elements of control.

Other than meteorology [29], DA tools are gaining popularity in different disciplines like reservoir engineering [30], and neuroscience [31]. Recent works have also drawn techniques and ideas from DA to enrich reduced order modeling

of fluid flows and vice versa [32–39]. In conventional projection-based model reduction approaches, a set of system’s realizations are used to build a reduced order model (ROM) that sufficiently represent the system’s dynamics with significantly lower computational cost [40–57]. This process includes the extraction of a handful of basis functions representing the underlying flow patterns or coherent structures that dominate the majority of the bulk mass, momentum and energy transfers. In fluid community, proper orthogonal decomposition (POD) is, generally speaking, the most popular and effective technique that produces hierarchically ordered solution-adapted basis functions (or modes) that provide the optimal basis to represent a given collection of field data or snapshots [50, 58–61]. To emulate system’s dynamics, a surrogate model is often built by performing a Galerkin projection of the full order model (FOM) operators onto a reduced subspace spanned by the formerly constructed POD modes [62–69].

However, the off-design performance of ROMs is usually questionable since the reduced basis and operators are formed offline for a given set of operating conditions, while the ROM has to be solved online for different conditions. Therefore, a dynamic update of model operators and parameters is often sought to enhance the applicability of ROMs in realistic contexts. That being said, adoption of DA tools to absorb real observations to correct and update ROMs should present a viable cure for this caveat. The present paper aims at pushing towards utilizing DA techniques to improve the performance of nonlinear ROMs. A common problem that emerges in such ROMs is the stability of solution, which is usually attributed to the modal truncation and intrinsic interactions between truncated modes and retained modes. In other words, the system’s nonlinearity implies that *all* the modes are coupled and strongly interact with each other. In ROM, we discard all but the first few modes and by enforcing this modal truncation, we eliminate the interactions between retained and truncated modes. This, in turn, gives rise to solution inaccuracies and instabilities. In order to address these issues, closure and stabilization techniques have been introduced to account for the effects of discarded modes on the dynamics of the ROM. In particular, eddy viscosity closures (inspired from large eddy simulations, LES) have shown a significant success in ROM closure modeling [32, 70–74]. The estimation of an optimal value of the eddy viscosity parameter has been the topic for many research works though. For example, empirical relations can be adopted [75–77], or ideas can be borrowed from LES to dynamically compute a better approximation of the eddy viscosity parameter [78–81]. Moreover, a 4D-VAR approach has been suggested to provide an optimal nonlinear eddy viscosity estimate in Galerkin projection based ROMs [32]. An adaptive nudging technique has also been recently introduced to force ROMs towards the reference solution corresponding to the observed data [33].

Instead, in the present paper, we propose a novel framework to estimate eddy viscosity closure using noisy observations from a sparse observation network. In particular, we adopt the forward sensitivity method to evaluate the sensitivity of ROM predictions to the eddy viscosity parameter. Observations, whenever available, can therefore be used to approximate a more representative value of eddy viscosity to better reflect the true system’s dynamics. We highlight that the proposed approach is very suitable for emerging digital twin applications [82–87], where real-time measurements are abundant (and noisy). Thus, efficiently assimilating these measurements to improve ROMs can be a key enabler for such applications which require many-query and near real-time simulations. We test our approach using the one-dimensional viscous Burgers equation with a square wave representing a moving shock. This problem is highly nonlinear, and therefore becomes challenging for standard Galerkin ROM (GROM) unless a large number of modes is used. We apply the proposed GROM-FSM to assimilate information from either full field or sparse field measurements. Therefore, our approach provides a modular framework to optimally estimate closure parameters for submodal scale physics, which can be effectively used in emerging sensor-centric applications in transport processes.

The rest of the paper is outlined here. In Section 2, we review the forward sensitivity method and its mathematical foundation as an established data assimilation algorithm. We then construct the standard Galerkin ROM and the corresponding reduced operators for the 1D Burgers problem in Section 3. Then, we describe the proposed approach for closure estimation via FSM, namely GROM-FSM, in Section 4. Results and relevant discussions are provided in Section 5. In particular, we consider the assimilation of full field and sparse field measurements. For the latter, we explore two approaches for assimilating information from sparse observations. Concluding remarks and insights are drawn in Section 6.

2 Forward Sensitivity Method

In this section, we briefly describe the forward sensitivity method (FSM) proposed by Lakshmivarahan and Lewis [27]. The idea behind this technique is to find optimal control parameters by iteratively correcting the control for the least squares fit of the model to the observational data. The control parameters in question here can be any unknown such as initial conditions, boundary conditions, and physical model parameters. The correction to each control parameter is dictated by its corresponding sensitivity function. In essence, the sensitivity function is the quantitative measure of influence of each control parameter on the model states. It is this nature of combining physical model with actual data to solve an inverse problem is what makes FSM a modular DA approach.

Let the dynamical system of interest be defined by a set of ordinary differential equations (ODEs) as below,

$$\frac{d\mathbf{x}}{dt} = \mathbf{f}(\mathbf{x}, \boldsymbol{\alpha}), \quad (1)$$

where $\mathbf{x}(t) \in \mathbb{R}^n$ is the system state-vector with the initial condition \mathbf{x}^0 and $\boldsymbol{\alpha} \in \mathbb{R}^p$ denotes the physical parameters. The vector of control parameters is represented as $\mathbf{c} = [\mathbf{x}^0, \boldsymbol{\alpha}]^T \in \mathbb{R}^{n+p}$. Here, it is assumed that the solution $\mathbf{x}(t)$ exists and is unique and has a smooth dependence with the control vector \mathbf{c} .

Discretizing Eq. 1 by using some numerical method like Runge-Kutta schemes, we get a model equation which gives the evolution of model states in discrete time as,

$$\mathbf{x}^{k+1} = \mathbf{M}(\mathbf{x}^k, \boldsymbol{\alpha}), \quad (2)$$

where $\mathbf{x}^k = [x_1^k, x_2^k, \dots, x_n^k]^T$ denotes the time-discretized model states at discrete time t_k and $\mathbf{M} = [M_1(\mathbf{x}^k, \boldsymbol{\alpha}), M_2(\mathbf{x}^k, \boldsymbol{\alpha}), \dots, M_n(\mathbf{x}^k, \boldsymbol{\alpha})]^T$ refer to the state transition maps from time t_k to t_{k+1} . Differentiating Eq. 2 with respect to \mathbf{x}^0 , we get

$$\frac{\partial x_i^{k+1}}{\partial x_j^0} = \sum_{q=1}^n \left(\frac{\partial M_i}{\partial x_q^k} \right) \left(\frac{\partial x_q^k}{\partial x_j^0} \right), \quad (3)$$

where $1 \leq i, j \leq n$. Similarly, differentiating Eq. 2 with respect to $\boldsymbol{\alpha}$, we obtain

$$\frac{\partial x_i^{k+1}}{\partial \alpha_j} = \sum_{q=1}^n \left(\frac{\partial M_i}{\partial x_q^k} \right) \left(\frac{\partial x_q^k}{\partial \alpha_j} \right) + \frac{\partial M_i}{\partial \alpha_j} \quad (4)$$

where $1 \leq i \leq n$ and $1 \leq j \leq p$. In Eq. 3 and Eq. 4, the superscript refers to the discrete time index while the subscript refers to the specific component. Now, we can define \mathbf{U}^k as the sensitivity matrix of \mathbf{x}^k with respect to initial state, where $[\mathbf{U}^k]_{ij} = \partial x_i^k / \partial x_j^0$ for $1 \leq i, j \leq n$. Also, we define \mathbf{V}^k as the sensitivity matrix of \mathbf{x}^k with respect to the parameter-vector $\boldsymbol{\alpha}$, where $[\mathbf{V}^k]_{ij} = \partial x_i^k / \partial \alpha_j$ for $1 \leq i \leq n$ and $1 \leq j \leq p$. Then, we can rewrite Eqs. 3-4 in matrix as below

$$\mathbf{U}^{k+1} = \mathbf{D}_{\mathbf{x}}^k(\mathbf{M})\mathbf{U}^k, \quad (5)$$

$$\mathbf{V}^{k+1} = \mathbf{D}_{\mathbf{x}}^k(\mathbf{M})\mathbf{V}^k + \mathbf{D}_{\boldsymbol{\alpha}}(\mathbf{M}), \quad (6)$$

initialized as $\mathbf{U}^0 = \mathbf{I}$ and $\mathbf{V}^0 = \mathbf{0}$.

Here, $\mathbf{D}_{\mathbf{x}}^k(\mathbf{M})$ and $\mathbf{D}_{\boldsymbol{\alpha}}(\mathbf{M})$ are the Jacobian matrices of $\mathbf{M}(\cdot)$ with respect to \mathbf{x} and $\boldsymbol{\alpha}$ at discrete time t_k , respectively. Moreover, $\mathbf{U}^k \in \mathbb{R}^{n \times n}$ and $\mathbf{V}^k \in \mathbb{R}^{n \times p}$ are called the forward sensitivity matrices with respect to initial conditions and parameters, respectively. In effect, the system dynamics in Eq. 2 gets reduced to a set of linear matrix equations (Eq. 5 and Eq. 6) which give the evolution of the sensitivity matrices in discrete time. By first order approximation, we have

$$\Delta \mathbf{x}^k \approx \delta \mathbf{x}^k = \mathbf{U}^k \delta \mathbf{x}^0 + \mathbf{V}^k \delta \boldsymbol{\alpha}, \quad (7)$$

where $\delta \mathbf{x} \in \mathbb{R}^n$.

So far, no observational data have been used. Let $\mathbf{z}(t) \in \mathbb{R}^m$ be the observation vector available for N time snapshots; and $\mathbf{h} : \mathbb{R}^n \rightarrow \mathbb{R}^m$ maps the model space \mathbb{R}^n to the observation space \mathbb{R}^m . Hence, the observation vector can be defined mathematically as follows,

$$\mathbf{z}(t) = \mathbf{h}(\tilde{\mathbf{x}}) + \mathbf{v}(t), \quad (8)$$

where $\tilde{\mathbf{x}} \in \mathbb{R}^n$ is the true state of the system and $\mathbf{v}(t) \in \mathbb{R}^m$ represents the measurement noise, which is assumed to be white Gaussian noise with zero mean and covariance matrix $\mathbf{R}(t) \in \mathbb{R}^{m \times m}$. Writing Eq. 8 in the discrete-time form we get,

$$\mathbf{z}^k = \mathbf{h}(\tilde{\mathbf{x}}^k) + \mathbf{v}^k, \quad (9)$$

where \mathbf{v}^k is white Gaussian noise with the covariance matrix \mathbf{R}^k . In most cases, \mathbf{R}^k is a diagonal matrix. For simplicity, we assume that $\mathbf{R}^k = \sigma_{Obs}^2 \mathbf{I}_m$, where \mathbf{I}_m is the $m \times m$ identity matrix.

Assuming that the model is perfect representation of the actual physical phenomenon and given a starting guess value of the control \mathbf{c} , we can run the model forward to predict $\mathbf{x}^k \forall 1 \leq k \leq N$, then the forecast error $\mathbf{e}_F^k \in \mathbb{R}^m$ defined as,

$$\mathbf{e}_F^k = \mathbf{z}^k - \mathbf{h}(\mathbf{x}^k). \quad (10)$$

The forecast error \mathbf{e}_F^k is composed of the sum of a deterministic part defined as $\mathbf{h}(\tilde{\mathbf{x}}^k) - \mathbf{h}(\mathbf{x}^k)$ and a random part \mathbf{v}^k . The random error stems from the inherent error in the mapping $\mathbf{h} : \mathbf{x}^k \rightarrow \mathbf{z}^k$ and we have no control on it, however it

is the goal of FSM to minimize the deterministic part in a least squares sense at all the N time snaps by choosing an optimal value for \mathbf{c} .

Now, the goal of FSM is to find a perturbation to the control $\delta\mathbf{c}$ from the given starting guess \mathbf{c} . This, in turn, would cause a $\delta\mathbf{x}^k$ change in \mathbf{x}^k such that the actual observation matches with the forecast observation from the model as follows,

$$\mathbf{z}^k = \mathbf{h}(\mathbf{x}^k + \delta\mathbf{x}^k) \approx \mathbf{h}(\mathbf{x}^k) + \mathbf{D}_{\mathbf{x}}^k(\mathbf{h})\delta\mathbf{x}^k. \quad (11)$$

Thus, the forecast error \mathbf{e}_F^k can be written as,

$$\mathbf{e}_F^k = \mathbf{D}_{\mathbf{x}}^k(\mathbf{h})\delta\mathbf{x}^k. \quad (12)$$

Combining Eq. 7 with Eq. 12, and setting $\mathbf{H}_1^k = \mathbf{D}_{\mathbf{x}}^k(\mathbf{h})\mathbf{U}^k \in \mathbb{R}^{m \times n}$, $\mathbf{H}_2^k = \mathbf{D}_{\mathbf{x}}^k(\mathbf{h})\mathbf{V}^k \in \mathbb{R}^{m \times p}$, we get,

$$\mathbf{e}_F^k = \mathbf{H}_1^k\delta\mathbf{x}^0 + \mathbf{H}_2^k\delta\alpha. \quad (13)$$

Equation 13 can be further simplified and written in terms of the perturbation to the control $\delta\mathbf{c}$ as

$$\mathbf{H}^k\delta\mathbf{c} = \mathbf{e}_F^k, \quad (14)$$

where $\mathbf{H}^k = [\mathbf{H}_1^k, \mathbf{H}_2^k] \in \mathbb{R}^{m \times (n+p)}$ and $\delta\mathbf{c} = [\delta\mathbf{x}^0, \delta\alpha]^T \in \mathbb{R}^{n+p}$.

Equation 14 can be formulated for all the N time snaps for which observations are available and the following linear equation is obtained,

$$\mathbf{H}\delta\mathbf{c} = \mathbf{e}_F, \quad (15)$$

where the matrix $\mathbf{H} \in \mathbb{R}^{Nm \times (n+p)}$ and the vector $\mathbf{e}_F \in \mathbb{R}^{Nm}$ are defined as follows,

$$\mathbf{H} = \begin{bmatrix} \mathbf{H}^1 \\ \mathbf{H}^2 \\ \vdots \\ \mathbf{H}^N \end{bmatrix}, \quad \mathbf{e}_F = \begin{bmatrix} \mathbf{e}_F^1 \\ \mathbf{e}_F^2 \\ \vdots \\ \mathbf{e}_F^N \end{bmatrix} \quad (16)$$

Depending on the value of Nm relative to $(n + p)$, Eq. 15 can give rise to either an over-determined or an under-determined linear inverse problem. In either case, the inverse problem can be solved in a weighted least squares sense to find an optimal value of $\delta\mathbf{c}$, with \mathbf{R}^{-1} as a weighting matrix, where \mathbf{R} is a block-diagonal matrix constructed as follows,

$$\mathbf{R} = \begin{bmatrix} \mathbf{R}^1 & & & \\ & \mathbf{R}^2 & & \\ & & \ddots & \\ & & & \mathbf{R}^N \end{bmatrix}. \quad (17)$$

For simplicity, we assume that \mathbf{R} is a diagonal matrix defined as $\mathbf{R} = \sigma_{Obs}^2 \mathbf{I}_{Nm}$, where \mathbf{I}_{Nm} is the $Nm \times Nm$ identity matrix. Then, the solution of Eq. 15 can be written as

$$\delta\mathbf{c} = \begin{cases} (\mathbf{H}^T \mathbf{R}^{-1} \mathbf{H})^{-1} \mathbf{H}^T \mathbf{R}^{-1} \mathbf{e}_F, & \text{over-determined,} \\ \mathbf{R}^{-1} \mathbf{H}^T (\mathbf{H} \mathbf{R}^{-1} \mathbf{H}^T)^{-1} \mathbf{e}_F, & \text{under-determined.} \end{cases} \quad (18)$$

It has been seen that the first order approximation progressively yield better results by repeating the entire process for multiple iterations until convergence with certain tolerance [27].

3 Reduced Order Modeling

In this section, we briefly derive a reduced order model (ROM) for the one-dimensional (1D) Burgers equation defined with the following partial differential equation (PDE)

$$\frac{\partial u}{\partial t} + u \frac{\partial u}{\partial x} = \nu \frac{\partial^2 u}{\partial x^2}, \quad (19)$$

where ν is the kinematic viscosity. In dimensionless form, ν is set as the reciprocal of Reynolds number, Re .

We follow the standard Galerkin projection to construct the sought ROM which includes two main steps. First, the velocity field $u(x, t)$ is approximated as a linear superposition of the contributions of a few modes, which can be mathematically expressed as

$$u(x, t) = \sum_{k=1}^R a_k(t) \phi_k(x), \quad (20)$$

where $\phi_k(x)$ are the spatial modes (or basis functions), $a_k(t)$ are the time-dependent modal coefficients (i.e., weighting functions), and R is the number of retained modes in ROM approximation (i.e., ROM dimension). Equation 20 is sometimes supplemented with an affine transformation, introducing a shift mode (e.g., a mean-field or equilibrium state), but here we adhere to the form given in Eq. 20 for simplicity and clarity of presentation. The second step is to project the governing equation (i.e., Eq. 19) onto the subspace spanned by $\{\phi_k\}_{k=1}^R$. Thus, the two main ingredients for building a Galerkin-based ROM (GROM) are the basis functions $\{\phi_k\}_{k=1}^R$ and a Galerkin projection of the governing equation. To compute the basis functions $\{\phi_k\}_{k=1}^R$, we follow the popular proper orthogonal decomposition (POD) approach described in Section 3.1, followed by derivation of GROM equations in Section 3.2.

3.1 Proper orthogonal decomposition

Proper orthogonal decomposition (POD) is data-driven modal decomposition technique that gained the highest popularity in fluid community due to its simplicity as well as robustness. Given a set of solution trajectories or realizations (known as snapshots), POD lays out a systematic approach to compute a solution-adapted basis functions that provide the optimal basis to represent a given set of simulation data or snapshots. Specifically, POD produces a hierarchically organized basis functions, based on their contribution to the total system's energy, which makes the modal selection a trivial process. In particular, given a collection of system realizations, we build a snapshot matrix $\mathbf{A} \in \mathbb{R}^{n \times N}$ as follows,

$$\mathbf{A} = \begin{bmatrix} u(x_1, t_1) & u(x_1, t_2) & \dots & u(x_1, t_N) \\ u(x_2, t_1) & u(x_2, t_2) & \dots & u(x_2, t_N) \\ \vdots & \vdots & \ddots & \vdots \\ u(x_n, t_1) & u(x_n, t_2) & \dots & u(x_n, t_N) \end{bmatrix}, \quad (21)$$

where n is the number of spatial locations and N is the number of snapshots. Then, a thin singular value decomposition (SVD) is performed on \mathbf{A} ,

$$\mathbf{A} = \mathbf{U} \Sigma \mathbf{V}^T, \quad (22)$$

where $\mathbf{U} \in \mathbb{R}^{n \times N}$ is a matrix with orthonormal columns are the left singular vectors of \mathbf{A} , which represent the spatial basis as,

$$\mathbf{U} = \begin{bmatrix} U_1(x_1) & U_2(x_1) & \dots & U_N(x_1) \\ U_1(x_2) & U_2(x_2) & \dots & U_N(x_2) \\ \vdots & \vdots & \ddots & \vdots \\ U_1(x_n) & U_2(x_n) & \dots & U_N(x_n) \end{bmatrix}, \quad (23)$$

while the columns of $\mathbf{V} \in \mathbb{R}^{N \times N}$ are the right singular vectors of \mathbf{A} , representing the temporal basis as

$$\mathbf{V} = \begin{bmatrix} V_1(t_1) & V_2(t_1) & \dots & V_N(t_1) \\ V_1(t_2) & V_2(t_2) & \dots & V_N(t_2) \\ \vdots & \vdots & \ddots & \vdots \\ V_1(t_N) & V_2(t_N) & \dots & V_N(t_N) \end{bmatrix}. \quad (24)$$

The singular values of \mathbf{A} are stored in descending order as the entries of the diagonal matrix $\Sigma \in \mathbb{R}^{N \times N}$,

$$\Sigma = \begin{bmatrix} \sigma_1 & & & \\ & \sigma_2 & & \\ & & \ddots & \\ & & & \sigma_N \end{bmatrix}, \quad (25)$$

where $\sigma_1 \geq \sigma_2 \geq \dots \geq \sigma_N \geq 0$. For dimensionality reduction purposes, only the first R columns of \mathbf{U} , corresponding to the largest R singular values, are stored. Those represent the most effective R POD modes, denoted as $\{\phi_k\}_{k=1}^R$ in the rest of the manuscript. The computed basis functions are orthonormal by construction as

$$\langle \phi_i; \phi_j \rangle = \begin{cases} 1 & \text{if } i = j \\ 0 & \text{otherwise,} \end{cases} \quad (26)$$

where the angle parentheses $\langle \cdot; \cdot \rangle$ stands for the standard inner product in Euclidean space (i.e., dot product). We note that the presented direct algorithm might be unfeasible for larger data sets, as stacking snapshots into a single huge matrix is usually prohibitive. Instead, the method of snapshots [58] can be followed to efficiently approximate the POD bases.

3.2 Galerkin ROM

Having a set of POD basis functions in hand, an orthogonal projection can be performed to obtain the Galerkin-based ROM (GROM). To do so, the ROM approximation (Eq. 20) is substituted into the governing equation (Eq. 19). Noting that the POD bases are only spatial functions (i.e., independent of time) and the modal coefficients are independent of space, we get the following,

$$\left(\sum_{i=1}^R \frac{\partial a_i}{\partial t} \phi_i \right) + \left(\sum_{i=1}^R a_i \phi_i \right) \left(\sum_{i=1}^R a_i \frac{\partial \phi_i}{\partial x} \right) = \nu \left(\sum_{i=1}^R a_i \frac{\partial^2 \phi_i}{\partial x^2} \right). \quad (27)$$

Then, an inner product with an arbitrary basis function ϕ_k is conducted, utilizing the orthonormality property of the basis function, which reduces $\sum_{i=1}^R \left\langle \frac{\partial a_i}{\partial t} \phi_i; \phi_k \right\rangle$ into $\frac{\partial a_k}{\partial t}$. After a few mathematical manipulations and *cleaning*, we get the following set of ordinary differential equations (ODEs) representing the tensorial GROM

$$\frac{da_k}{dt} = \nu \sum_{i=1}^R \mathfrak{L}_{i,k} a_i + \sum_{i=1}^R \sum_{j=1}^R \mathfrak{N}_{i,j,k} a_i a_j, \quad (28)$$

where \mathfrak{L} and \mathfrak{N} are the matrix and tensor of predetermined model coefficients corresponding to linear and nonlinear terms, respectively. They are precomputed during an offline stage as

$$\begin{aligned} \mathfrak{L}_{i,k} &= \left\langle \frac{\partial^2 \phi_i}{\partial x^2}; \phi_k \right\rangle, \\ \mathfrak{N}_{i,j,k} &= \left\langle -\phi_i \frac{\partial \phi_j}{\partial x}; \phi_k \right\rangle. \end{aligned}$$

Due to the quadratic nonlinearity in the system, the computational cost of solving Eq. 28 is $O(R^3)$. Therefore, the number of retained modes has to be reduced as much as possible to keep the computational cost affordable. However, this truncation ignores the dyadic interactions between the first R modes and the remaining ones. As a result, instabilities arise in the ROM solution [88–90], and closure/stabilization techniques need to be introduced to improve ROM accuracy [32, 72–74, 76, 78, 91–101].

4 Closure Estimation via FSM

In order to stabilize the GROM, a closure model is usually necessary for complex flows. In the present paper, we consider adding an eddy-viscosity term to Eq. 19 as follows,

$$\frac{\partial u}{\partial t} + u \frac{\partial u}{\partial x} = (\nu + \nu_e) \frac{\partial^2 u}{\partial x^2}, \quad (29)$$

where ν is the physical (kinematic) viscosity and ν_e is an (artificial) eddy viscosity to add an extra dissipation to stabilize the system. If we follow the same procedure in Section 3.2, we get the following GROM with closure,

$$\frac{da_k}{dt} = (\nu + \nu_e) \sum_{i=1}^R \mathfrak{L}_{i,k} a_i + \sum_{i=1}^R \sum_{j=1}^R \mathfrak{N}_{i,j,k} a_i a_j. \quad (30)$$

It remains to compute or assume a good estimate for ν_e . Using an a priori estimate for ν_e can produce a stable ROM solution. However, as the flow evolves, this prior value might become less effective. Therefore, there should be a strategy to dynamically update this estimate based on the flow conditions/regimes.

In this regard, we borrow ideas from meteorological data assimilation to correct and update our parameter estimate using live and realistic (possibly noisy) measurements. In particular, we use the forward sensitivity method (FSM), described in Section 2, to compute an optimal value for eddy viscosity given a few field observations. This also allows us to update our estimate whenever a new observation is available. We start with a prior estimate of eddy viscosity

(e.g., zero if no priors are available), and solve the ROM equation for a given period of time, T_w . As we solve GROM, we also collect some field measurements during this period T_w . A penalty term is thus computed as the difference between the GROM prediction and observations, which is used to update our prior estimate for ν_e . This updated value is therefore used to evolve the GROM until new observations become available to match with model's predictions, and so on. The period over which measurements are collected T_w is called the data assimilation window. Note that model's states (e.g., $a_k(t)$) can be different from the measured quantities (e.g., $u(x, t)$), and a mapping between model space and observation space has to be defined. In the following, we formalize our framework for FSM-based eddy viscosity estimation for GROM, called GROM-FSM in the present study. Defining our dynamic model as

$$\frac{d\mathbf{a}}{dt} = \mathbf{f}(\mathbf{a}, \nu_e), \quad (31)$$

where \mathbf{a} is the vector of modal coefficients defined as $\mathbf{a} = [a_1, a_2, \dots, a_R]^T$ (the superscript T denotes transpose). The (time-continuous) model map \mathbf{f} is defined as follows,

$$\mathbf{f} = \begin{bmatrix} (\nu + \nu_e) \sum_{i=1}^R \mathfrak{L}_{i,1} a_i + \sum_{i=1}^R \sum_{j=1}^R \mathfrak{N}_{i,j,1} a_i a_j \\ (\nu + \nu_e) \sum_{i=1}^R \mathfrak{L}_{i,2} a_i + \sum_{i=1}^R \sum_{j=1}^R \mathfrak{N}_{i,j,2} a_i a_j \\ \vdots \\ (\nu + \nu_e) \sum_{i=1}^R \mathfrak{L}_{i,R} a_i + \sum_{i=1}^R \sum_{j=1}^R \mathfrak{N}_{i,j,R} a_i a_j \end{bmatrix}.$$

A time-discretization scheme can be utilized to convert this model from continuous-time map \mathbf{f} to a discrete-time map \mathbf{M} as

$$\mathbf{a}^{k+1} = \mathbf{M}(\mathbf{a}^k, \nu_e), \quad (32)$$

where the superscript k denotes the time index. In our implementation, we adopt the fourth-order Runge-Kutta scheme (RK4) for temporal discretization.

Suppose we collect measurements \mathbf{z}^k at a single time instant t_k , where $t_k \in [0, T_w]$. The forecast error is defined at t_k as

$$\mathbf{e}_F^k = \mathbf{z}^k - \mathbf{h}(\mathbf{a}^k), \quad (33)$$

where $\mathbf{h}(\cdot)$ defines the mapping from model space to observation space. In our results, we consider two mapping cases. In the first case, we preprocess field observations to compute the “observed” coefficients (i.e., $\mathbf{z}^k = \mathbf{a}_{Obs}^k$), where the mapping is simply identity matrix (i.e., $\mathbf{h}(\mathbf{a}^k) = \mathbf{a}^k$). In the second case, we keep observations as velocity field measurement ($\mathbf{z}^k = \mathbf{u}_{Obs}^k$), where the mapping becomes a reconstruction map (i.e., $\mathbf{h}(\mathbf{a}^k) = \mathbf{u}^k$). Specific details are to be given in Section 5.

Although the FSM can be used to treat uncertainties in initial conditions as well as model parameters, we only consider the estimation of the eddy viscosity parameter ν_e . Thus,

$$\mathbf{H}_2^k \delta \nu_e = \mathbf{e}_F^k, \quad (34)$$

where $\mathbf{H}_2^k = \mathbf{D}_{\mathbf{a}}^k(\mathbf{h}) \mathbf{V}^k$ as defined in Section 2. Details of defining model Jacobian are given in **Appendix A**. For more than a single observation time, we stack Eq. 34 at different observation times to get the following equation,

$$\mathbf{H}_2 \delta \nu_e = \mathbf{e}_F. \quad (35)$$

Also, a block-diagonal matrix \mathbf{R} is constituted with the measurement covariance matrices \mathbf{R}^k at subsequent observation times. Equation 35 defines an over-determined system of linear equations in $\delta \nu_e$. A weighted least-squares solution can be computed, with a weighting matrix of \mathbf{R}^{-1} as follows,

$$\delta \nu_e = (\mathbf{H}_2^T \mathbf{R}^{-1} \mathbf{H}_2)^{-1} \mathbf{H}_2^T \mathbf{R}^{-1} \mathbf{e}_F, \quad (36)$$

where $\delta \nu_e$ is added to our prior estimate of ν_e (also called background) to obtain a better approximation and the process is repeated until convergence. The procedure for using FSM to compute the eddy viscosity is summarized in Algorithm 1. We note that an initial guess for eddy viscosity parameter is required for proper implementation of the

algorithm. If no prior knowledge of ν_e is available, a zero initial guess usually works fine. Also, a tolerance limit has to be set to define convergence (e.g., 1×10^{-6}).

Algorithm 1: Forward sensitivity method for estimating eddy viscosity in GROM closure

Input : Dynamic model $M(\cdot)$, observation operator $h(\cdot)$, initial condition a^1 , a set of observations z^1, z^2, \dots, z^N , an initial guess for eddy viscosity parameter ν_e , and a tolerance tol value

Output : An estimate of the eddy viscosity ν_e

initialization

for $i \leftarrow 1$ **to** $max\ iter$ **do**

$$V^1 = 0$$

$$e_F = z^1 - h(a^1)$$

$$H_2 = D_a^1(h)V^1$$

$$R = R^1$$

for $n \leftarrow 1$ **to** $N - 1$ **do**

$$a^{n+1} = M(a^n, \nu_e)$$

$$V^{n+1} = D_a^n(M)V^n + D_{\nu_e}(M)$$

if (observation z^{n+1} is available) **then**

$$e_F^{n+1} = z^{n+1} - h(a^{n+1})$$

$$H_2^{n+1} = D_a^{n+1}(h)V^{n+1}$$

$$e_F = \begin{bmatrix} e_F \\ e_F^{n+1} \end{bmatrix}, \quad H_2 = \begin{bmatrix} H_2 \\ H_2^{n+1} \end{bmatrix}$$

$$R = \begin{bmatrix} R & \\ & R^{n+1} \end{bmatrix}$$

end

end

$$\delta\nu_e = (H_2^T R^{-1} H_2)^{-1} H_2^T R^{-1} e_F$$

if ($\delta\nu_e \leq tol$) **then**

 | *break*

else

$$| \quad \nu_e = \nu_e + \delta\nu_e$$

end

end

5 Results

We test the proposed methodology for computing and updating the eddy viscosity parameter via FSM on the 1D Burgers problem. In particular, we assume an initial condition of a square wave defined as

$$u(x, 0) = \begin{cases} 1, & \text{if } 0 < x \leq L/2 \\ 0, & \text{if } L/2 < x \leq L, \end{cases} \quad (37)$$

with zero Dirichlet boundary conditions, $u(0, t) = u(L, t) = 0$. We consider a spatial domain of $L = 1$, and solve at $Re = 10^4$ for $t \in [0, 1]$. For numerical computations, we use a family of fourth order compact schemes for spatial derivatives [102], and skew-symmetric formulation for the nonlinear term. Also, we use the fourth order Runge-Kutta (RK4) scheme for temporal integration with a time step of 10^{-4} over a spatial grid of 4096. For POD basis generation, we collect 100 snapshots (i.e., every 100 time steps). The temporal evolution of the 1D Burgers problem using the described setup is shown in Figure 1, where we can see the advection of the shock wave.

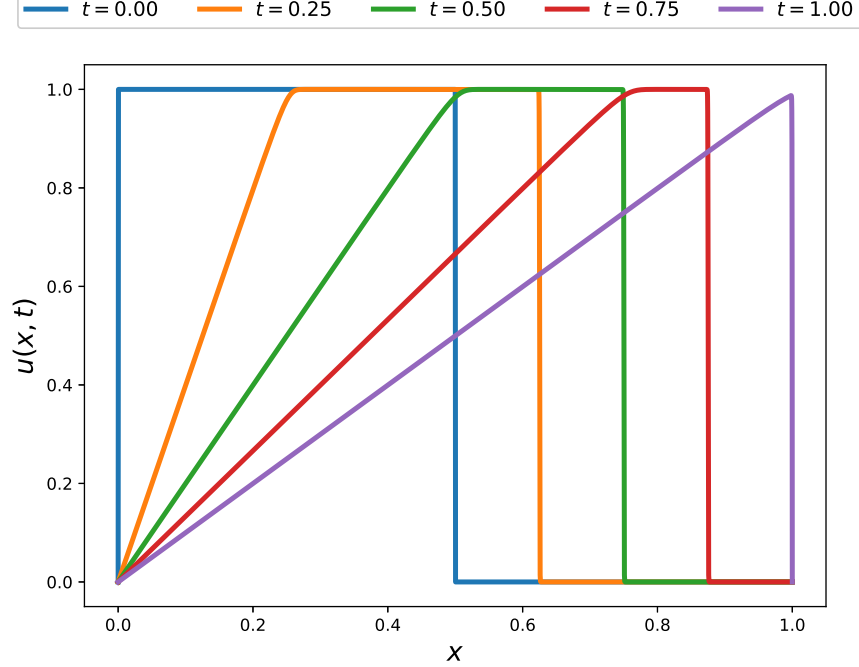


Figure 1: Evolution of the FOM velocity field, characterized by a moving shock with square wave.

The described Burgers problem with square wave is challenging for ROM applications. In our GROM implementation, we consider $R = 8$ modes and $\Delta t = 0.01$ for time integration. In the following, we discuss the estimation of eddy viscosity via FSM using full and sparse field measurements.

5.1 Full field measurement

In our first case, we investigate the assimilation of noisy full field measurement as

$$u_{Obs}(x, t) = u(x, t) + v(x, t), \quad (38)$$

where $v(x, t)$ is a white Gaussian noise with zero mean and covariance matrix $\mathbf{R}(t)$. In particular, we define $\mathbf{R}(t) = \sigma_{Obs}^2 \mathbf{I}$, with $\sigma_{Obs} = 0.1$. We assume a data assimilation window of 0.5 s and collect measurements at $t = 0.25$ and $t = 0.5$, as demonstrated in Figure 2.

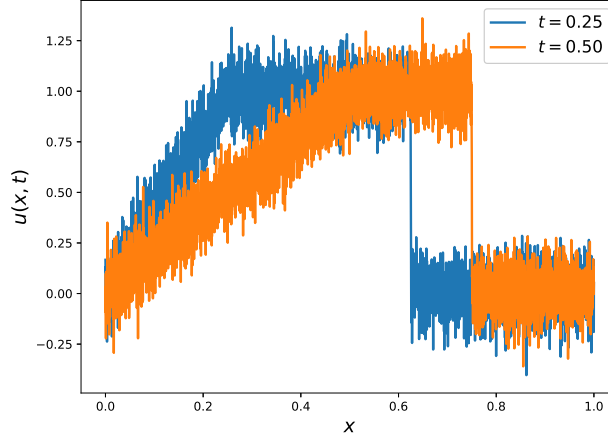


Figure 2: Noisy measurement of velocity fields at $t = 0.25$ s and $t = 0.5$ s, assuming sensors are located at all grid points.

Instead of defining a map between model space and observation space, we preprocess our measurement by projecting them onto the POD basis to compute the ‘‘observed’’ modal coefficients as

$$a_{i,Obs}^k = \langle \mathbf{u}_{Obs}^k; \phi_i \rangle. \quad (39)$$

Thus, $\mathbf{z}^k = \mathbf{a}_{Obs}$ and the observation operator is defined $\mathbf{h}(\mathbf{a}) = \mathbf{a}$, with a Jacobian of identity matrix (i.e., $\mathbf{D}_a(\mathbf{h}) = \mathbf{I}_R$, where \mathbf{I}_R is the $R \times R$ identity matrix). Also, the observational covariance matrix is set as $\mathbf{R}^k = \sigma_{Obs}^2 \mathbf{I}_R$. If we implement the procedure described in Section 2 to obtain an estimate for ν_e and solve GROM with and without closure, we obtain the results in Figure 3 for the temporal evolution the modal coefficients. For comparison, we also plot the true projection values of \mathbf{a} , defined as

$$a_i^k = \langle \mathbf{u}_{FOM}^k; \phi_i \rangle. \quad (40)$$

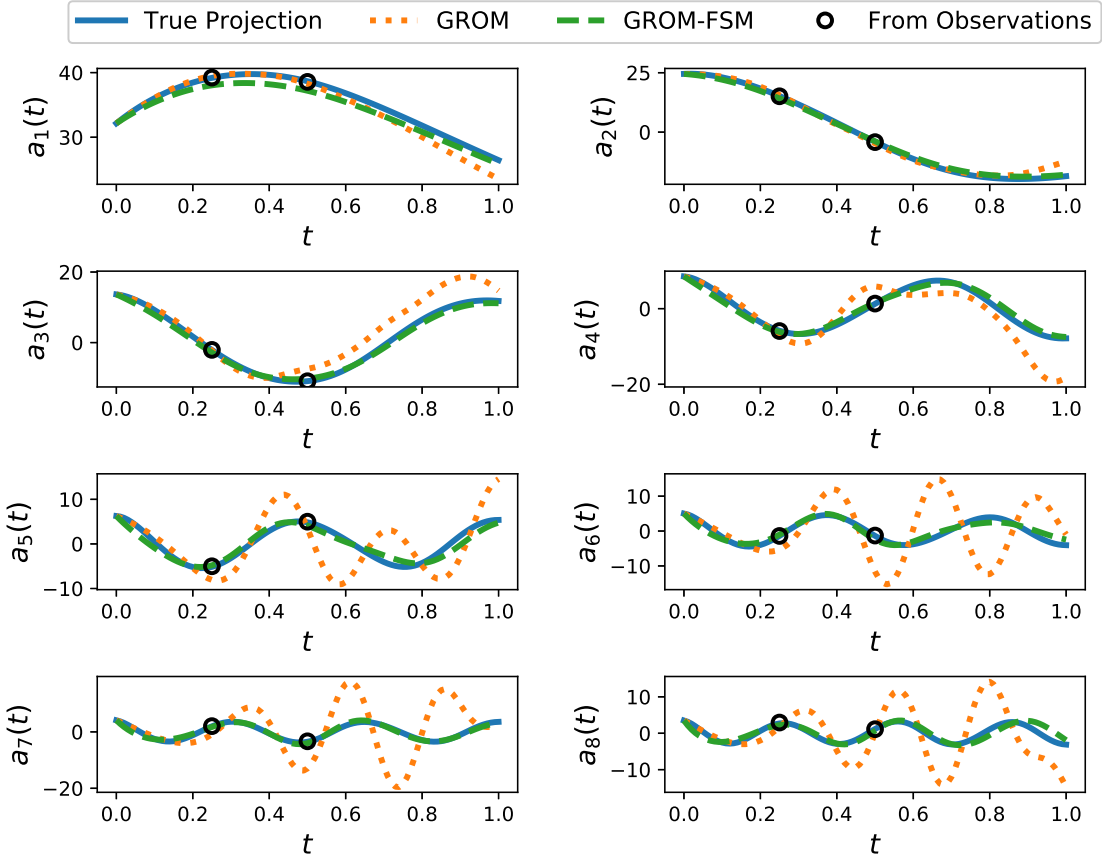


Figure 3: Temporal evolution of POD coefficients, assuming full field measurements are available.

Also, we sketch reconstructed velocity field at final time $t = 1$ in Figure 3. It is clear that GROM without closure is unable to capture the true dynamical behavior of the described Burgers problem. On the other hand, GROM-FSM is shown to almost match the true projection. It is assumed that true projected values represent the best values that projection-based ROM can provide. For quantitative assessment, we also plot the root mean squares error of ROM predictions defined as

$$RMSE(t) = \sqrt{\frac{1}{n} \sum_{i=1}^n \left(u_{FOM}(x_i, t) - u_{ROM}(x_i, t) \right)^2} \quad (41)$$

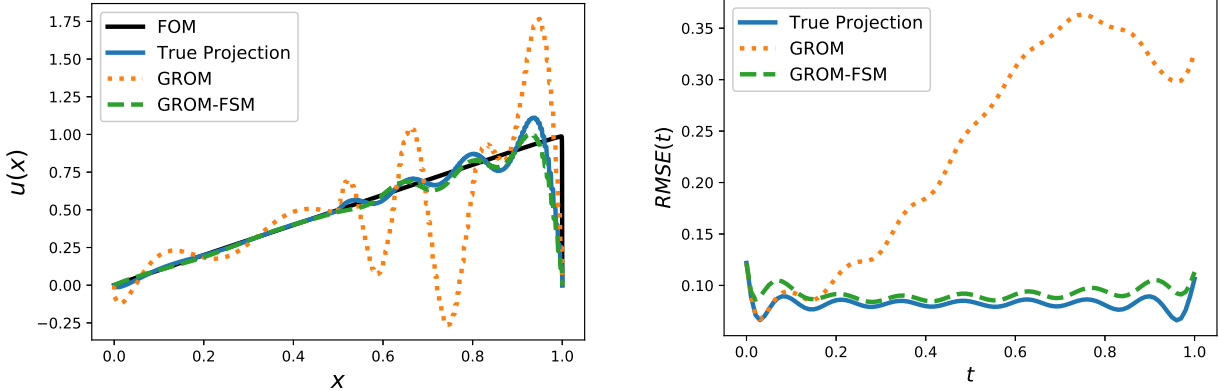


Figure 4: Velocity field reconstruction in case of full field measurements. Left: reconstruction of final velocity field using GROM and GROM with FSM eddy viscosity compared to the FOM and true projection fields. Right: RMSE of reconstructed fields at different time instants.

5.2 Sparse field measurement

Since full field measurements are usually inaccessible, we extend our study to consider sparse field measurements. In particular, we locate sensors at 8 points, equally spaced at $1/8, 2/8, 3/8, 4/8, 5/8, 6/8, 7/8, 8/8$ as shown in Figure 5. To assimilate those measurements, we consider two cases. The first one is similar to the full field measurement case, where we preprocess those measurements to compute a least-squares approximation of the corresponding observed modal coefficients. In the second case, we keep our observation as field measurements and define an operator to map model state (i.e., modal coefficients) to observations (i.e., velocity).

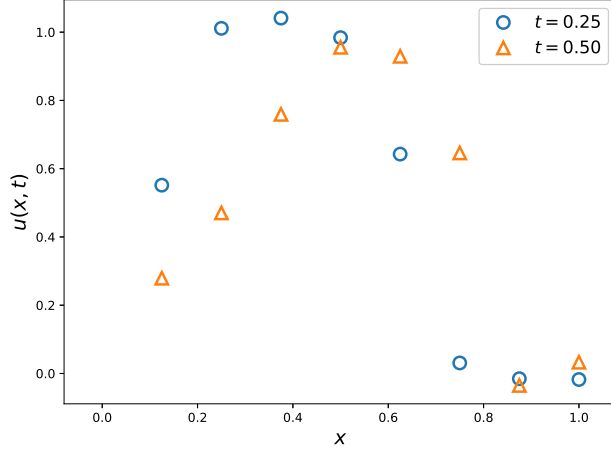


Figure 5: Noisy measurement of velocity fields at $t = 0.25$ s and $t = 0.50$ s, assuming sensors are located at 8 grid points.

5.2.1 From measurements to POD coefficients

In order to preprocess the sparse measurements to approximate the observed modal coefficients, we sample Eq. 20 at the sensors locations as follows,

$$\begin{bmatrix} \phi_1(x_{O1}) & \phi_2(x_{O1}) & \dots & \phi_R(x_{O1}) \\ \phi_1(x_{O2}) & \phi_2(x_{O2}) & \dots & \phi_R(x_{O2}) \\ \vdots & & & \vdots \\ \phi_1(x_{O8}) & \phi_2(x_{O8}) & \dots & \phi_R(x_{O8}) \end{bmatrix} \begin{bmatrix} a_{1,Obs}^k \\ a_{2,Obs}^k \\ \vdots \\ a_{R,Obs}^k \end{bmatrix} = \begin{bmatrix} u_{Obs}^k(x_{O1}) \\ u_{Obs}^k(x_{O2}) \\ \vdots \\ u_{Obs}^k(x_{O8}) \end{bmatrix}, \quad (42)$$

which can be generally solved using the pseudo-inverse. Then, the same observation operator and its Jacobian as defined in Section 5.1 are used. The temporal evolution of the modal coefficients are given in Figure 6. Although the GROM-FSM results are better than GROM, they are significantly worse than those in Figure 3. Of course, this is to be expected since we are using measurements at only 8 points, rather than 4096 locations. However, we also find that the observed modal coefficients calculations using Eq. 42 is greatly sensitive to the level of noise. Indeed, we find that least-squares computations sometimes do not converge (a remedy will be provided in Section 5.2.2). Moreover, we can see that the POD modal coefficients from observations are significantly different than the true ones.

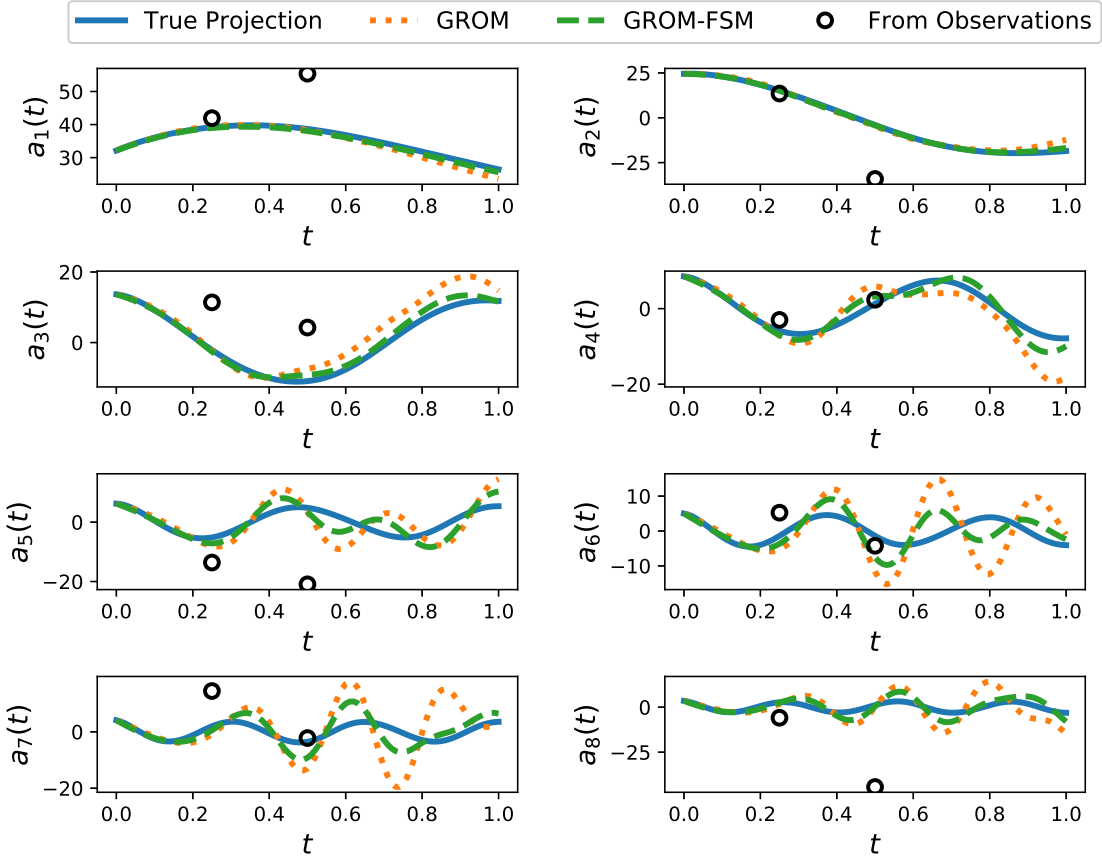


Figure 6: Temporal evolution of POD coefficients, where sparse field measurements are preprocessed to estimate the observed POD coefficients.

The reconstructed field at final time as well as the *RMSE* at different times are demonstrated in Figure 7. We see that a small improvement is obtained in GROM-FSM, compared to GROM. We also note that for different noise levels, we get different performances for the GROM-FSM. This implies that this way of assimilating sparse observations is less reliable, and a more robust approach should be utilized. In Section 5.2.2, we discuss another way of using sparse observations to perform data assimilation for ROM closure.

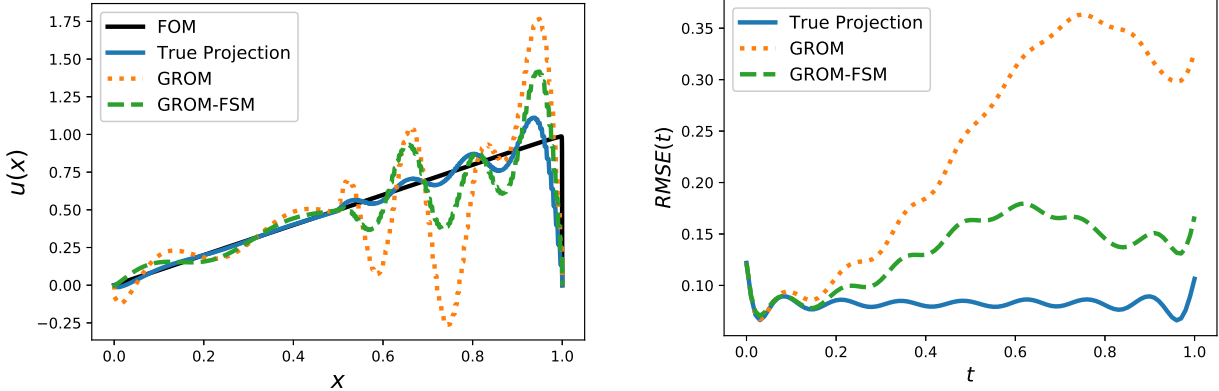


Figure 7: Velocity field reconstruction in case of preprocessing sparse field measurements to compute the observed POD coefficients. Left: reconstruction of final velocity field using GROM and GROM with FSM eddy viscosity compared to the FOM and true projection fields. Right: RMSE of reconstructed fields at different time instants.

5.2.2 From POD coefficients to measurements

Now, we discuss defining an observational operator to construct a robust map between model space and measurement space. Similar to Section 5.2.1, we sample Eq. 20 at sensor location, but we introduce a map to reconstruct the velocity field at these locations using the model predicted coefficients. In other words, in Section 5.2.1, we use the sensors measurements to approximate a value for \mathbf{a}_{Obs}^k . But in this section, we use model predicted coefficients \mathbf{a}^k to approximate the velocity field values at sensor locations (i.e., $u^k(x_{O1}), u^k(x_{O2}), \dots, u^k(x_{O8})$) as follows,

$$\begin{bmatrix} \phi_1(x_{O1}) & \phi_2(x_{O1}) & \dots & \phi_R(x_{O1}) \\ \phi_1(x_{O2}) & \phi_2(x_{O2}) & \dots & \phi_R(x_{O2}) \\ \vdots & & & \vdots \\ \phi_1(x_{O8}) & \phi_2(x_{O8}) & \dots & \phi_R(x_{O8}) \end{bmatrix} \begin{bmatrix} a_1^k \\ a_2^k \\ \vdots \\ a_R^k \end{bmatrix} = \begin{bmatrix} u^k(x_{O1}) \\ u^k(x_{O2}) \\ \vdots \\ u^k(x_{O8}) \end{bmatrix}. \quad (43)$$

Thus, we define $\mathbf{z}^k = \mathbf{u}_{Obs}^k$, and the observation operator $\mathbf{h}(\mathbf{a}) = \mathbf{C}\mathbf{a}$, where \mathbf{C} is the matrix of basis functions sampled at sensors locations as follows,

$$\mathbf{C} = \begin{bmatrix} \phi_1(x_{O1}) & \phi_2(x_{O1}) & \dots & \phi_R(x_{O1}) \\ \phi_1(x_{O2}) & \phi_2(x_{O2}) & \dots & \phi_R(x_{O2}) \\ \vdots & & & \vdots \\ \phi_1(x_{O8}) & \phi_2(x_{O8}) & \dots & \phi_R(x_{O8}) \end{bmatrix}. \quad (44)$$

Thus, the Jacobian of $\mathbf{h}(\cdot)$ is defined as $\mathbf{D}_\mathbf{a}(\mathbf{h}) = \mathbf{C}$. We repeat the same GROM-FSM implementation with those redefined operators. Results are shown in Figure 8 and Figure 9, where we can see that this approach of assimilating measurements is more robust than the one discussed in Section 5.2.1 with higher accuracy. We also note that similar performance is achieved using higher level of noise in measurements, while the approach in Section 5.2.1 requires very low level of observational noise.

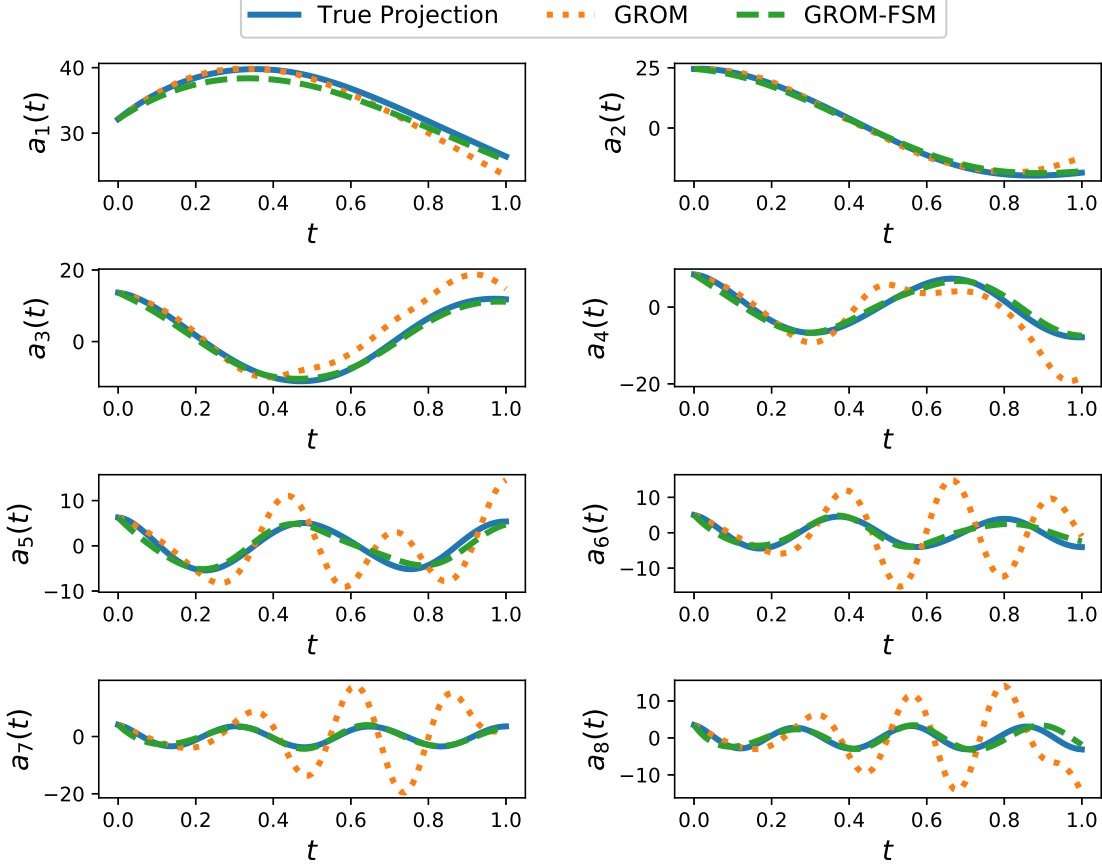


Figure 8: Temporal evolution of POD coefficients, where sparse field measurements are compared against POD field reconstruction using the observer operator \mathbf{C} .

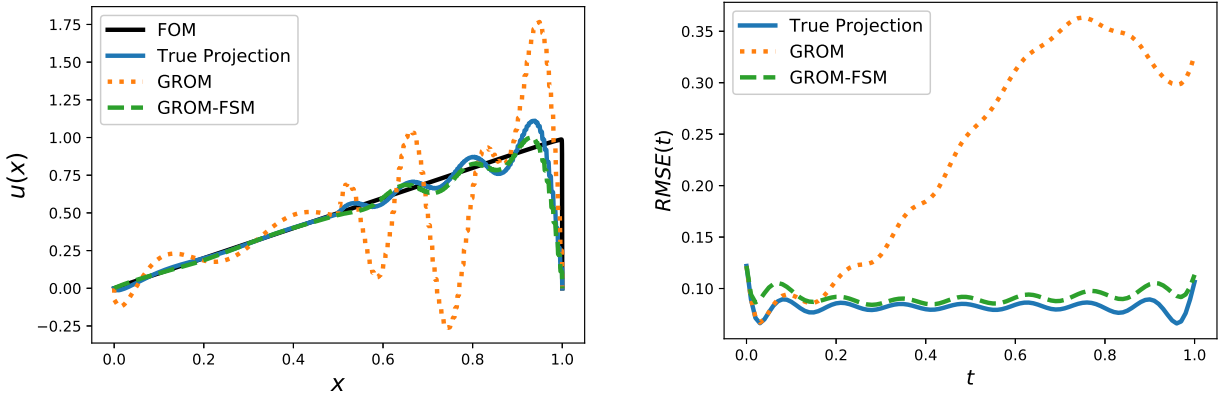


Figure 9: Velocity field reconstruction where sparse field measurements are compared against POD field reconstruction using the observer operator \mathbf{C} . Left: reconstruction of final velocity field using GROM and GROM with FSM eddy viscosity compared to the FOM and true projection fields. Right: RMSE of reconstructed fields at different time instants.

Finally, for a big picture comparison, we plot the spatio-temporal evolution of reconstructed velocity fields for all discussed measurement setups compared to FOM and true projection fields in Figure 10. From this figure, we notice

that solution of GROM without closure is unstable, and brings non-physical predictions. On the other hand, predictions of GROM-FSM with full field measurements almost match the true projected fields. Also, assimilating sparse observations via the reconstruction map C is significantly superior to approximating observed coefficients using the pseudo-inverse approach. The latter shows some non-physical predictions, similar to GROM.

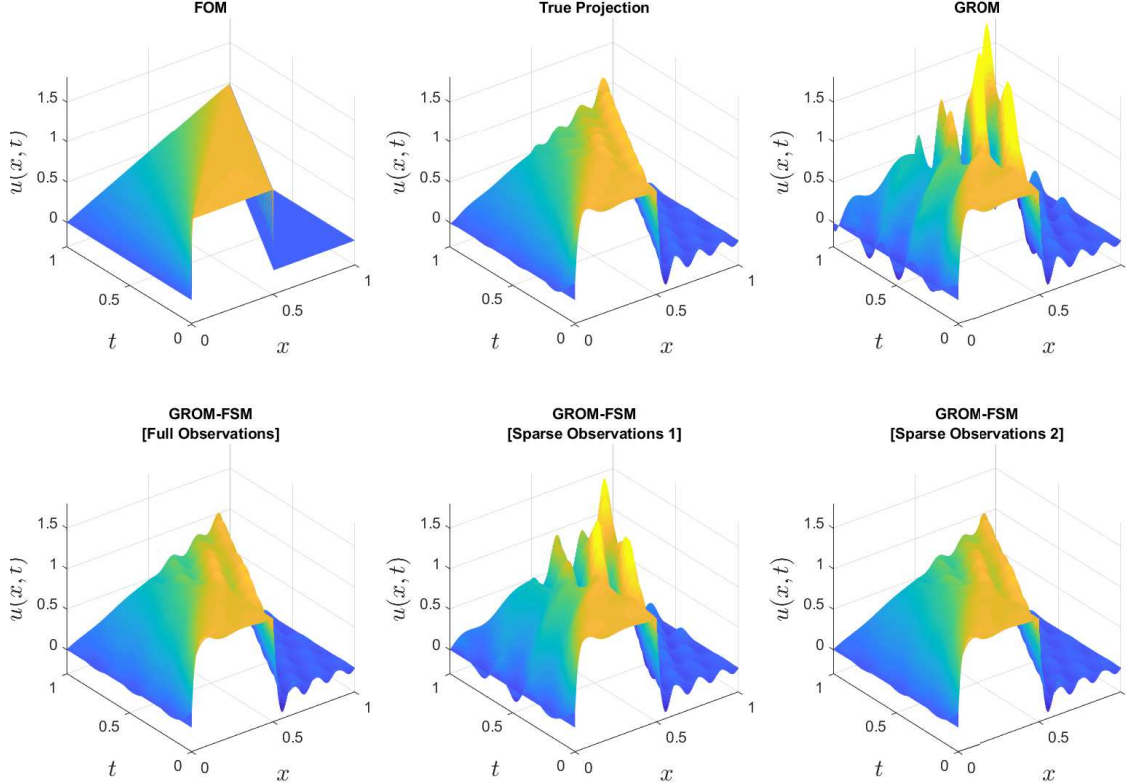


Figure 10: Surface plots for the temporal evolution of velocity fields from FOM, true projection, GROM and FSM with different observations configurations. Note: Sparse Observation 1 refers to the method presented in Section 5.2.1, while Sparse Observation 2 refers to the method presented in Section 5.2.2.

6 Concluding Remarks

In the present study, we propose a data assimilation-based approach to provide accurate ROMs for digital twin applications. In particular, we use the forward sensitivity method (FSM) to estimate as well as update an optimal value of eddy viscosity for ROM closure. We exploit ongoing streams of observational data to improve the stability and accuracy of ROM predictions. We test the framework with the prototypical one-dimensional viscous Burgers equation, characterized by strong non-linearity. We investigate the assimilation of full field and sparse field measurements. For full field measurements, we illustrate that projecting those noisy measurements produces good estimate of *observed* modal coefficients, which can therefore be used to estimate an optimal value for eddy viscosity. However, we find that a similar approach of using sparse field measurements to approximate the observed states is significantly sensitive to measurements noise. On the other hand, we demonstrate that defining an observational operator via a ROM reconstruction map can be successful in utilizing sparse and noisy data. Using real-time observations can steer ROM parameters and predictions to reflect actual flow conditions. We emphasize that fusing ideas between physics-based closures (e.g., the ansatz for eddy viscosity) and model reduction with variational data assimilation techniques can provide valuable tools to construct reliable ROMs for long-time as well off-design predictions. This should leverage ROM implementation for real-life application.

Acknowledgements

We thank Sivaramakrishnan Lakshmivarahan for his insightful comments as well as his archival NPTEL lectures that greatly helped us in understanding the mechanics of the FSM method. This material is based upon work supported by the U.S. Department of Energy, Office of Science, Office of Advanced Scientific Computing Research under Award Number de-sc0019290. O.S. gratefully acknowledges their support.

Disclaimer: This report was prepared as an account of work sponsored by an agency of the United States Government. Neither the United States Government nor any agency thereof, nor any of their employees, makes any warranty, express or implied, or assumes any legal liability or responsibility for the accuracy, completeness, or usefulness of any information, apparatus, product, or process disclosed, or represents that its use would not infringe privately owned rights. Reference herein to any specific commercial product, process, or service by trade name, trademark, manufacturer, or otherwise does not necessarily constitute or imply its endorsement, recommendation, or favoring by the United States Government or any agency thereof. The views and opinions of authors expressed herein do not necessarily state or reflect those of the United States Government or any agency thereof.

References

- [1] Michael Ghil and Paola Malanotte-Rizzoli. Data assimilation in meteorology and oceanography. In *Advances in Geophysics*, volume 33, pages 141–266. Elsevier, 1991.
- [2] Eugenia Kalnay. *Atmospheric modeling, data assimilation and predictability*. Cambridge University Press, Cambridge, 2003.
- [3] John M Lewis, Sivaramakrishnan Lakshmivarahan, and Sudarshan Dhall. *Dynamic data assimilation: a least squares approach*, volume 104. Cambridge University Press, Cambridge, 2006.
- [4] Andrew C Lorenc. Analysis methods for numerical weather prediction. *Quarterly Journal of the Royal Meteorological Society*, 112(474):1177–1194, 1986.
- [5] David F Parrish and John C Derber. The national meteorological center’s spectral statistical-interpolation analysis system. *Monthly Weather Review*, 120(8):1747–1763, 1992.
- [6] Philippe Courtier. Dual formulation of four-dimensional variational assimilation. *Quarterly Journal of the Royal Meteorological Society*, 123(544):2449–2461, 1997.
- [7] Florence Rabier, Heikki Järvinen, E Klinker, J-F Mahfouf, and A Simmons. The ECMWF operational implementation of four-dimensional variational assimilation. I: Experimental results with simplified physics. *Quarterly Journal of the Royal Meteorological Society*, 126(564):1143–1170, 2000.
- [8] Hendrik Elbern, H Schmidt, O Talagrand, and Adolf Ebel. 4D-variational data assimilation with an adjoint air quality model for emission analysis. *Environmental Modelling & Software*, 15(6-7):539–548, 2000.
- [9] PHILIPPE Courtier, J-N Thépaut, and Anthony Hollingsworth. A strategy for operational implementation of 4D-Var, using an incremental approach. *Quarterly Journal of the Royal Meteorological Society*, 120(519):1367–1387, 1994.
- [10] Andrew C Lorenc and F Rawlins. Why does 4D-Var beat 3D-Var? *Quarterly Journal of the Royal Meteorological Society*, 131(613):3247–3257, 2005.
- [11] Pierre Gauthier, Monique Tanguay, Stephane Laroche, Simon Pellerin, and Josee Morneau. Extension of 3DVAR to 4DVAR: Implementation of 4dvar at the meteorological service of Canada. *Monthly Weather Review*, 135(6):2339–2354, 2007.
- [12] Peter L Houtekamer and Herschel L Mitchell. Data assimilation using an ensemble Kalman filter technique. *Monthly Weather Review*, 126(3):796–811, 1998.
- [13] Gerrit Burgers, Peter Jan van Leeuwen, and Geir Evensen. Analysis scheme in the ensemble Kalman filter. *Monthly Weather Review*, 126(6):1719–1724, 1998.
- [14] Geir Evensen. The ensemble Kalman filter: Theoretical formulation and practical implementation. *Ocean Dynamics*, 53(4):343–367, 2003.
- [15] Peter L Houtekamer and Herschel L Mitchell. A sequential ensemble Kalman filter for atmospheric data assimilation. *Monthly Weather Review*, 129(1):123–137, 2001.
- [16] Peter L Houtekamer and Herschel L Mitchell. Ensemble kalman filtering. *Quarterly Journal of the Royal Meteorological Society: A journal of the atmospheric sciences, applied meteorology and physical oceanography*, 131(613):3269–3289, 2005.

- [17] Dimitri Treebushny and Henrik Madsen. A new reduced rank square root Kalman filter for data assimilation in mathematical models. In *International Conference on Computational Science*, pages 482–491. Springer, 2003.
- [18] Mark Buehner and Paola Malanotte-Rizzoli. Reduced-rank Kalman filters applied to an idealized model of the wind-driven ocean circulation. *Journal of Geophysical Research: Oceans*, 108(C6), 2003.
- [19] S Lakshmivarahan and David J Stensrud. Ensemble Kalman filter. *IEEE Control Systems Magazine*, 29(3):34–46, 2009.
- [20] Milija Zupanski. Maximum likelihood ensemble filter: Theoretical aspects. *Monthly Weather Review*, 133(6):1710–1726, 2005.
- [21] Gérald Desroziers, Jean-Thomas Camino, and Loïk Berre. 4DEnVar: link with 4D state formulation of variational assimilation and different possible implementations. *Quarterly Journal of the Royal Meteorological Society*, 140(684):2097–2110, 2014.
- [22] Andrew C Lorenc, Neill E Bowler, Adam M Clayton, Stephen R Pring, and David Fairbairn. Comparison of hybrid-4DEnVar and hybrid-4DVar data assimilation methods for global NWP. *Monthly Weather Review*, 143(1):212–229, 2015.
- [23] Xuguang Wang, Dale M Barker, Chris Snyder, and Thomas M Hamill. A hybrid ETKF–3DVAR data assimilation scheme for the WRF model. Part I: Observing system simulation experiment. *Monthly Weather Review*, 136(12):5116–5131, 2008.
- [24] M Buehner, J Morneau, and C Charette. Four-dimensional ensemble-variational data assimilation for global deterministic weather prediction. *Nonlinear Processes in Geophysics*, 20(5), 2013.
- [25] Daryl T Kleist and Kayo Ide. An OSSE-based evaluation of hybrid variational–ensemble data assimilation for the NCEP GFS. Part I: System description and 3D-hybrid results. *Monthly Weather Review*, 143(2):433–451, 2015.
- [26] Daryl T Kleist and Kayo Ide. An OSSE-based evaluation of hybrid variational–ensemble data assimilation for the NCEP GFS. Part II: 4DEnVar and hybrid variants. *Monthly Weather Review*, 143(2):452–470, 2015.
- [27] S Lakshmivarahan and John M Lewis. Forward sensitivity approach to dynamic data assimilation. *Advances in Meteorology*, 2010:1–12, 2010.
- [28] Sivaramakrishnan Lakshmivarahan, John M Lewis, and Rafal Jabrzemski. *Forecast error correction using dynamic data assimilation*. Springer, Switzerland, 2017.
- [29] Bin Wang, Xiaolei Zou, and Jiang Zhu. Data assimilation and its applications. *Proceedings of the National Academy of Sciences*, 97(21):11143–11144, 2000.
- [30] Sigurd I Aanonsen, Geir Nævdal, Dean S Oliver, Albert C Reynolds, Brice Vallès, et al. The ensemble kalman filter in reservoir engineering—a review. *SPE Journal*, 14(03):393–412, 2009.
- [31] Axel Hutt and Roland Potthast. Forecast of spectral features by ensemble data assimilation. *Frontiers in Applied Mathematics and Statistics*, 4:52, 2018.
- [32] Bartosz Protas, Bernd R Noack, and Jan Östh. Optimal nonlinear eddy viscosity in Galerkin models of turbulent flows. *Journal of Fluid Mechanics*, 766:337–367, 2015.
- [33] Camille Zerfas, Leo G Rebholz, Michael Schneier, and Traian Iliescu. Continuous data assimilation reduced order models of fluid flow. *Computer Methods in Applied Mechanics and Engineering*, 357:112596, 2019.
- [34] D Xiao, J Du, F Fang, CC Pain, and J Li. Parameterised non-intrusive reduced order methods for ensemble Kalman filter data assimilation. *Computers & Fluids*, 177:69–77, 2018.
- [35] Dacian N Daescu and I Michael Navon. Efficiency of a POD-based reduced second-order adjoint model in 4D-Var data assimilation. *International Journal for Numerical Methods in Fluids*, 53(6):985–1004, 2007.
- [36] Răzvan Ștefănescu, Adrian Sandu, and Ionel Michael Navon. POD/DEIM reduced-order strategies for efficient four dimensional variational data assimilation. *Journal of Computational Physics*, 295:569–595, 2015.
- [37] Yanhua Cao, Jiang Zhu, I Michael Navon, and Zhendong Luo. A reduced-order approach to four-dimensional variational data assimilation using proper orthogonal decomposition. *International Journal for Numerical Methods in Fluids*, 53(10):1571–1583, 2007.
- [38] Céline Robert, S Durbiano, Eric Blayo, Jacques Verron, Jacques Blum, and F-X Le Dimet. A reduced-order strategy for 4d-var data assimilation. *Journal of Marine Systems*, 57(1-2):70–82, 2005.
- [39] Rossella Arcucci, Laetitia Mottet, Christopher Pain, and Yi-Ke Guo. Optimal reduced space for variational data assimilation. *Journal of Computational Physics*, 379:51–69, 2019.

[40] Zhaojun Bai. Krylov subspace techniques for reduced-order modeling of large-scale dynamical systems. *Applied Numerical Mathematics*, 43(1-2):9–44, 2002.

[41] David J Lucia, Philip S Beran, and Walter A Silva. Reduced-order modeling: new approaches for computational physics. *Progress in Aerospace Sciences*, 40(1-2):51–117, 2004.

[42] Martin Hess, Alessandro Alla, Annalisa Quaini, Gianluigi Rozza, and Max Gunzburger. A localized reduced-order modeling approach for PDEs with bifurcating solutions. *Computer Methods in Applied Mechanics and Engineering*, 351:379–403, 2019.

[43] Boris Kramer and Karen E Willcox. Nonlinear model order reduction via lifting transformations and proper orthogonal decomposition. *AIAA Journal*, 57(6):2297–2307, 2019.

[44] Renee Swischuk, Laura Mainini, Benjamin Peherstorfer, and Karen Willcox. Projection-based model reduction: Formulations for physics-based machine learning. *Computers & Fluids*, 179:704–717, 2019.

[45] Jake Bouvrie and Boumediene Hamzi. Kernel methods for the approximation of nonlinear systems. *SIAM Journal on Control and Optimization*, 55(4):2460–2492, 2017.

[46] Boumediene Hamzi and Eyad H Abed. Local modal participation analysis of nonlinear systems using Poincaré linearization. *Nonlinear Dynamics*, pages 1–9, 2019.

[47] Milan Korda, Mihai Putinar, and Igor Mezić. Data-driven spectral analysis of the Koopman operator. *Applied and Computational Harmonic Analysis*, 48:599–629, 2020.

[48] Milan Korda and Igor Mezić. Linear predictors for nonlinear dynamical systems: Koopman operator meets model predictive control. *Automatica*, 93:149–160, 2018.

[49] Dirk Hartmann, Matthias Herz, and Utz Wever. Model order reduction a key technology for digital twins. In *Reduced-Order Modeling (ROM) for Simulation and Optimization*, pages 167–179. Springer, 2018.

[50] Philip Holmes, John L Lumley, Gahl Berkooz, and Clarence W Rowley. *Turbulence, coherent structures, dynamical systems and symmetry*. Cambridge University Press, Cambridge, 2012.

[51] Kunihiko Taira, Steven L Brunton, Scott TM Dawson, Clarence W Rowley, Tim Colonius, Beverley J McKeon, Oliver T Schmidt, Stanislav Gordeyev, Vassilios Theoflis, and Lawrence S Ukeiley. Modal analysis of fluid flows: An overview. *AIAA Journal*, pages 4013–4041, 2017.

[52] Kunihiko Taira, Maziar S Hemati, Steven L Brunton, Yiyang Sun, Karthik Duraisamy, Shervin Bagheri, Scott TM Dawson, and Chi-An Yeh. Modal analysis of fluid flows: Applications and outlook. *AIAA Journal*, pages 1–25, 2019.

[53] Bernd R Noack, Marek Morzynski, and Gilead Tadmor. *Reduced-order modelling for flow control*, volume 528. Springer, Berlin, 2011.

[54] Clarence W Rowley and Scott TM Dawson. Model reduction for flow analysis and control. *Annual Review of Fluid Mechanics*, 49:387–417, 2017.

[55] Nirmal J Nair and Maciej Balajewicz. Transported snapshot model order reduction approach for parametric, steady-state fluid flows containing parameter-dependent shocks. *International Journal for Numerical Methods in Engineering*, 117(12):1234–1262, 2019.

[56] Eurika Kaiser, Bernd R Noack, Laurent Cordier, Andreas Spohn, Marc Segond, Markus Abel, Guillaume Daviller, Jan Östh, Siniša Krajnović, and Robert K Niven. Cluster-based reduced-order modelling of a mixing layer. *Journal of Fluid Mechanics*, 754:365–414, 2014.

[57] Bernard Haasdonk, Markus Dihlmann, and Mario Ohlberger. A training set and multiple bases generation approach for parameterized model reduction based on adaptive grids in parameter space. *Mathematical and Computer Modelling of Dynamical Systems*, 17(4):423–442, 2011.

[58] Lawrence Sirovich. Turbulence and the dynamics of coherent structures. I. Coherent structures. *Quarterly of Applied Mathematics*, 45(3):561–571, 1987.

[59] Gal Berkooz, Philip Holmes, and John L Lumley. The proper orthogonal decomposition in the analysis of turbulent flows. *Annual Review of Fluid Mechanics*, 25(1):539–575, 1993.

[60] Anindya Chatterjee. An introduction to the proper orthogonal decomposition. *Current Science*, pages 808–817, 2000.

[61] Muruhan Rathinam and Linda R Petzold. A new look at proper orthogonal decomposition. *SIAM Journal on Numerical Analysis*, 41(5):1893–1925, 2003.

[62] Kazufumi Ito and Sivaguru S Ravindran. A reduced-order method for simulation and control of fluid flows. *Journal of Computational Physics*, 143(2):403–425, 1998.

[63] Angelo Iollo, Stéphane Lanteri, and J-A Désidéri. Stability properties of POD-Galerkin approximations for the compressible Navier-Stokes equations. *Theoretical and Computational Fluid Dynamics*, 13(6):377–396, 2000.

[64] Clarence W Rowley, Tim Colonius, and Richard M Murray. Model reduction for compressible flows using POD and Galerkin projection. *Physica D: Nonlinear Phenomena*, 189(1-2):115–129, 2004.

[65] René Milk, Stephan Rave, and Felix Schindler. pyMOR—generic algorithms and interfaces for model order reduction. *SIAM Journal on Scientific Computing*, 38(5):S194–S216, 2016.

[66] Vladimir Puzyrev, Mehdi Ghommem, and Shiv Meka. pyROM: A computational framework for reduced order modeling. *Journal of Computational Science*, 30:157–173, 2019.

[67] Michel Bergmann, C-H Bruneau, and Angelo Iollo. Enablers for robust POD models. *Journal of Computational Physics*, 228(2):516–538, 2009.

[68] M Couplet, C Basdevant, and P Sagaut. Calibrated reduced-order POD-Galerkin system for fluid flow modelling. *Journal of Computational Physics*, 207(1):192–220, 2005.

[69] Karl Kunisch and Stefan Volkwein. Galerkin proper orthogonal decomposition methods for parabolic problems. *Numerische Mathematik*, 90(1):117–148, 2001.

[70] Jeff Borggaard, Traian Iliescu, and Zhu Wang. Artificial viscosity proper orthogonal decomposition. *Mathematical and Computer Modelling*, 53(1-2):269–279, 2011.

[71] Zhu Wang, Imran Akhtar, Jeff Borggaard, and Traian Iliescu. Two-level discretizations of nonlinear closure models for proper orthogonal decomposition. *Journal of Computational Physics*, 230(1):126–146, 2011.

[72] Imran Akhtar, Zhu Wang, Jeff Borggaard, and Traian Iliescu. A new closure strategy for proper orthogonal decomposition reduced-order models. *Journal of Computational and Nonlinear Dynamics*, 7(3):034503, 2012.

[73] Laurent Cordier, Bernd R Noack, Gilles Tissot, Guillaume Lehnasch, Joel Delville, Maciej Balajewicz, Guillaume Daviller, and Robert K Niven. Identification strategies for model-based control. *Experiments in Fluids*, 54(8):1580, 2013.

[74] Omer San and Traian Iliescu. A stabilized proper orthogonal decomposition reduced-order model for large scale quasigeostrophic ocean circulation. *Advances in Computational Mathematics*, 41(5):1289–1319, 2015.

[75] D. Rempfer. *Kohärente Strukturen und Chaos beim laminar-turbulenten Grenzschichtumschlag*. PhD thesis, University of Stuttgart, 1997.

[76] Omer San and Traian Iliescu. Proper orthogonal decomposition closure models for fluid flows: Burgers equation. *International Journal of Numerical Analysis & Modeling. Series B*, 5:217–237, 2014.

[77] Mansoor Ahmed and Omer San. Stabilized principal interval decomposition method for model reduction of nonlinear convective systems with moving shocks. *Computational and Applied Mathematics*, 37(5):6870–6902, 2018.

[78] Zhu Wang, Imran Akhtar, Jeff Borggaard, and Traian Iliescu. Proper orthogonal decomposition closure models for turbulent flows: A numerical comparison. *Computer Methods in Applied Mechanics and Engineering*, 237:10–26, 2012.

[79] Sk M Rahman, Shady E Ahmed, and Omer San. A dynamic closure modeling framework for model order reduction of geophysical flows. *Physics of Fluids*, 31(4):046602, 2019.

[80] Changhong Mou, Birgul Koc, Omer San, and Traian Iliescu. Data-driven variational multiscale reduced order models. *arXiv preprint arXiv:2002.06457*, 2020.

[81] Haroon Imtiaz and Imran Akhtar. Nonlinear closure modeling in reduced order models for turbulent flows: a dynamical system approach. *Nonlinear Dynamics*, 99(1):479–494, 2020.

[82] Fei Tao, Jiangfeng Cheng, Qinglin Qi, Meng Zhang, He Zhang, and Fangyuan Sui. Digital twin-driven product design, manufacturing and service with big data. *The International Journal of Advanced Manufacturing Technology*, 94(9-12):3563–3576, 2018.

[83] Fei Tao, He Zhang, Ang Liu, and Andrew YC Nee. Digital twin in industry: State-of-the-art. *IEEE Transactions on Industrial Informatics*, 15(4):2405–2415, 2018.

[84] Azad M Madni, Carla C Madni, and Scott D Lucero. Leveraging digital twin technology in model-based systems engineering. *Systems*, 7(1):7, 2019.

[85] Adil Rasheed, Omer San, and Trond Kvamsdal. Digital twin: Values, challenges and enablers from a modeling perspective. *IEEE Access*, 8:21980–22012, 2020.

[86] R Ganguli and S Adhikari. The digital twin of discrete dynamic systems: Initial approaches and future challenges. *Applied Mathematical Modelling*, 77:1110–1128, 2020.

[87] Souvik Chakraborty, Sondipon Adhikari, and Ranjan Ganguli. The role of surrogate models in the development of digital twins of dynamic systems. *arXiv preprint arXiv:2001.09292*, 2020.

[88] Toni Lassila, Andrea Manzoni, Alfio Quarteroni, and Gianluigi Rozza. Model order reduction in fluid dynamics: challenges and perspectives. In *Reduced Order Methods for Modeling and Computational Reduction*, pages 235–273. Springer, 2014.

[89] D Rempfer. On low-dimensional Galerkin models for fluid flow. *Theoretical and Computational Fluid Dynamics*, 14(2):75–88, 2000.

[90] Bernd R Noack, Konstantin Afanasiev, Marek Morzynski, Gilead Tadmor, and Frank Thiele. A hierarchy of low-dimensional models for the transient and post-transient cylinder wake. *Journal of Fluid Mechanics*, 497:335–363, 2003.

[91] Sirod Sirisup and George E Karniadakis. A spectral viscosity method for correcting the long-term behavior of POD models. *Journal of Computational Physics*, 194(1):92–116, 2004.

[92] Omer San and Jeff Borggaard. Basis selection and closure for POD models of convection dominated Boussinesq flows. In *21st International Symposium on Mathematical Theory of Networks and Systems*, volume 5, 2014.

[93] Jan Östh, Bernd R Noack, Siniša Krajnović, Diogo Barros, and Jacques Borée. On the need for a nonlinear subscale turbulence term in POD models as exemplified for a high-reynolds-number flow over an Ahmed body. *Journal of Fluid Mechanics*, 747:518–544, 2014.

[94] M Couplet, P Sagaut, and C Basdevant. Intermodal energy transfers in a proper orthogonal decomposition–Galerkin representation of a turbulent separated flow. *Journal of Fluid Mechanics*, 491:275–284, 2003.

[95] Virginia L Kalb and Anil E Deane. An intrinsic stabilization scheme for proper orthogonal decomposition based low-dimensional models. *Physics of Fluids*, 19(5):054106, 2007.

[96] I Kalashnikova and MF Barone. On the stability and convergence of a Galerkin reduced order model (ROM) of compressible flow with solid wall and far-field boundary treatment. *International Journal for Numerical Methods in Engineering*, 83(10):1345–1375, 2010.

[97] Xuping Xie, Muhammad Mohebujjaman, Leo G Rebholz, and Traian Iliescu. Data-driven filtered reduced order modeling of fluid flows. *SIAM Journal on Scientific Computing*, 40(3):B834–B857, 2018.

[98] Muhammad Mohebujjaman, Leo G Rebholz, and Traian Iliescu. Physically constrained data-driven correction for reduced-order modeling of fluid flows. *International Journal for Numerical Methods in Fluids*, 89(3):103–122, 2019.

[99] Maciej Balajewicz and Earl H Dowell. Stabilization of projection-based reduced order models of the Navier–Stokes. *Nonlinear Dynamics*, 70(2):1619–1632, 2012.

[100] David Amsallem and Charbel Farhat. Stabilization of projection-based reduced-order models. *International Journal for Numerical Methods in Engineering*, 91(4):358–377, 2012.

[101] M Gunzburger, T Iliescu, M Mohebujjaman, and M Schneier. An evolve-filter-relax stabilized reduced order stochastic collocation method for the time-dependent Navier–Stokes equations. *SIAM/ASA Journal on Uncertainty Quantification*, 7(4):1162–1184, 2019.

[102] Sanjiva K Lele. Compact finite difference schemes with spectral-like resolution. *Journal of Computational Physics*, 103(1):16–42, 1992.

Appendix A: Computing Model Jacobians

For temporal discretization of the GROM equations, we use fourth-order Runge–Kutta (RK4) method as follows,

$$\mathbf{a}^{k+1} = \mathbf{a}^k + \frac{\Delta t}{6}(\mathbf{g}_1 + 2\mathbf{g}_2 + 2\mathbf{g}_3 + \mathbf{g}_4),$$

where

$$\begin{aligned}\mathbf{g}_1 &= \mathbf{f}(\mathbf{a}^k, \nu_e), \\ \mathbf{g}_2 &= \mathbf{f}\left(\mathbf{a}^k + \frac{\Delta t}{2} \cdot \mathbf{g}_1, \nu_e\right), \\ \mathbf{g}_3 &= \mathbf{f}\left(\mathbf{a}^k + \frac{\Delta t}{2} \cdot \mathbf{g}_2, \nu_e\right), \\ \mathbf{g}_4 &= \mathbf{f}(\mathbf{a}^k + \Delta t \cdot \mathbf{g}_3, \nu_e).\end{aligned}$$

Thus the discrete-time map defining the transition from time t_k to time t_{k+1} is written as

$$\mathbf{M}(\mathbf{a}^k, \nu_e) = \mathbf{a}^n + \frac{\Delta t}{6}(\mathbf{g}_1 + 2\mathbf{g}_2 + 2\mathbf{g}_3 + \mathbf{g}_4).$$

Then, the ‘total’ Jacobian of \mathbf{M} is an $R \times (R+1)$ matrix, computed as

$$\begin{aligned}\mathbf{D}^k(\mathbf{M}) &= [\mathbf{D}_{\mathbf{a}}^k(\mathbf{M}), \mathbf{D}_{\nu_e}^k(\mathbf{M})] \\ &= \mathbf{P} + \frac{\Delta t}{6} \left(\mathbf{D}\mathbf{g}_1 + 2\mathbf{D}\mathbf{g}_2 + 2\mathbf{D}\mathbf{g}_3 + \mathbf{D}\mathbf{g}_4 \right),\end{aligned}$$

where $\mathbf{P} = [\mathbf{I}_R, \mathbf{0}_{R \times 1}] \in \mathbb{R}^{R \times (R+1)}$. The Jacobian of the model \mathbf{M} with respect to the model state \mathbf{a}^k is the first R columns of $\mathbf{D}(\mathbf{M})$, while the Jacobian of \mathbf{M} with respect to the eddy viscosity parameter ν_e is the last column of $\mathbf{D}(\mathbf{M})$.

Here, $\mathbf{D}\mathbf{g}_1$, $\mathbf{D}\mathbf{g}_2$, $\mathbf{D}\mathbf{g}_3$, and $\mathbf{D}\mathbf{g}_4$ are evaluated using the chain rule as follows,

$$\begin{aligned}\mathbf{D}\mathbf{g}_1 &= \mathbf{D}\mathbf{f}(\mathbf{a}^k, \nu_e), \\ \mathbf{D}\mathbf{g}_2 &= \left(\mathbf{D}\mathbf{f}\left(\mathbf{a}^k + \frac{\Delta t}{2} \cdot \mathbf{g}_1, \nu_e\right) \right) \left(\mathbf{I}_{(R+1)} + \frac{\Delta t}{2} \begin{bmatrix} \mathbf{D}\mathbf{g}_1 \\ \mathbf{Q} \end{bmatrix} \right), \\ \mathbf{D}\mathbf{g}_3 &= \left(\mathbf{D}\mathbf{f}\left(\mathbf{a}^k + \frac{\Delta t}{2} \cdot \mathbf{g}_2, \nu_e\right) \right) \left(\mathbf{I}_{(R+1)} + \frac{\Delta t}{2} \begin{bmatrix} \mathbf{D}\mathbf{g}_2 \\ \mathbf{Q} \end{bmatrix} \right), \\ \mathbf{D}\mathbf{g}_4 &= \left(\mathbf{D}\mathbf{f}(\mathbf{a}^k + \Delta t \cdot \mathbf{g}_3, \nu_e) \right) \left(\mathbf{I}_{(R+1)} + \Delta t \begin{bmatrix} \mathbf{D}\mathbf{g}_3 \\ \mathbf{Q} \end{bmatrix} \right),\end{aligned}$$

where $\mathbf{Q} = \mathbf{0}_{1 \times (R+1)}$. Finally, the Jacobian of $\mathbf{D}\mathbf{f}(\mathbf{a}^k, \nu_e)$ is defined as $\mathbf{D}\mathbf{f}(\mathbf{a}^k, \nu_e) = [\mathbf{D}_{\mathbf{a}}\mathbf{f}(\mathbf{a}^k, \nu_e), \mathbf{D}_{\nu_e}\mathbf{f}(\mathbf{a}^k, \nu_e)]$, where

$$\begin{aligned}\frac{\partial f_k}{\partial a_j} &= (\nu + \nu_e) \mathfrak{L}_{j,k} + \sum_{i=1}^R \mathfrak{N}_{i,j,k} a_i + \sum_{i=1}^R \mathfrak{N}_{j,i,k} a_i, \\ \frac{\partial f_k}{\partial \nu_e} &= \sum_{i=1}^R \mathfrak{L}_{i,k} a_i,\end{aligned}$$

for $1 \leq j, k \leq R$.